

Time-resolved optical conductivity and Higgs oscillations in two-band dirty superconductors

Rafael Haenel,^{1,2} Paul Froese,^{1,2} Dirk Manske,¹ and Lukas Schwarz¹

¹*Max Planck Institute for Solid State Research, 70569 Stuttgart, Germany*

²*Quantum Matter Institute, University of British Columbia, Vancouver V6T 1Z4, Canada*

(Dated: November 4, 2020)

...

I. INTRODUCTION

When a global symmetry is spontaneously broken, collective excitations emerge. In the case of a superconductor, where the local order parameter $\Delta e^{i\varphi}$ acquires a finite value below a critical temperature T_C , two bosonic modes appear: the massive Higgs mode and a massless Goldstone mode. They may be seen as longitudinal and phase fluctuations of the complex order parameter in a Mexican hat free energy. In the presence of Coulomb interaction, the Goldstone mode is shifted to optical frequencies by means of the Anderson Higgs mechanism while the Higgs mode remains a stable gapped excitation in the Terahertz regime.

In a two-band superconductor, two gapless Higgs modes and two phase modes exist. While the global phase fluctuations occur only at energies close to the plasma frequency, relative phase fluctuations, termed Leggett mode, persist as a gapped excitation at low energies.

Experimental observation of Higgs and Leggett collective modes is difficult. Since the Higgs field is a scalar quantity, no linear coupling to the vectorial electromagnetic field can exist. Thus, there are no direct experimental signatures in linear response and experiments need to be performed in the non-linear regime. Here, the challenge is twofold: intense light sources are required but experiments also have to be performed on energy scales mostly within the superconducting gap such that optical excitation of quasiparticles does not deplete the condensate.

Recent developments in ultrafast Terahertz spectroscopy have caused a surge in interest in collective excitations in superconductors and experimental signatures of the Higgs mode have now been observed in various materials.

Experiments performed so far consist of two approaches. First, samples are illuminated in a pump-probe setup where an excitation of the Higgs mode by a single-cycle THz pump appears as an oscillation of the probe signal as a function of pump-probe delay. In a second type of experiments, the Higgs mode is resonantly driven by an intense multi-cycle pulse that yields a electrical field component of three times the pump frequency in the reflected or transmitted beam. Theoretically, time-resolved oscillation of the gap in angle-resolved photoemission (ARPES) spectra has also been studied as a third characterization scheme. Additionally, Higgs excitation has been proposed as its own spectroscopic method based on the insight

that the gap symmetry of a superconductor can be classified from measurements of the condensate oscillations in different geometries.

The fact that characteristics of the Higgs boson in superconductors are observable in experiments at all was not obvious from the beginning. Initially theoretical calculations in the clean limit predicted extremely weak experimental signatures unobservable with even today's experimental equipment. Only recently the role of impurities has been appreciated in achieving more realistic theoretical predictions. [list publications: Silaev, Murotani, Benfatto] In the clean limit, the Higgs mode only diamagnetically couples to the gauge field. Presence of impurities additionally enables a paramagnetic coupling which becomes the dominant contribution even for small disorder. It was further shown that impurity scattering yields qualitatively different behavior in the polarization dependence of the pump pulses.

An outstanding question MgB₂. Murotani. Demler experiment.

[How does this paper go beyond the work of Murotani and Shimano?]

- time resolved optical conductivity
- discussion of the second gap of MgB₂ - why can't we see it in optical experiment?
- Third harmonic generation where pulse frequency is swept. (todo: also sweep the temperature, show decomposition in terms of QP, Higgs, Leggett mode)
 - (Discussion of four cases)
- Coupling of Higgs and Leggett mode. Do they actually couple?
- Presentation using SI units to make everything easily comparable to experiments.
- Discussion of the paramagnetic activation in terms of diagrams?

This article is organized as follows. In Sec. II we briefly review key aspects of the model as introduced by Murotani and Shimano []. We then discuss the case of a single-band superconductor in a pump-probe scenario in Sec. III and make reference to available experimental data. In Sec. IV we study in detail the case of a two-band superconductor motivated by material parameters of MgB₂ with different impurity concentrations of the conduction bands. We summarize all results in Sec. V.

II. MODEL

A. Hamiltonian

We consider a meanfield description of a multiband s-wave BCS superconductor,

$$\mathcal{H}_0 = \sum_{i\mathbf{k}\sigma} \varepsilon_{i\mathbf{k}} c_{i\mathbf{k}\sigma}^\dagger c_{i\mathbf{k}\sigma} + \sum_{i\mathbf{k}} \left(\Delta_i c_{i-\mathbf{k}\uparrow}^\dagger c_{i\mathbf{k}\downarrow}^\dagger \right), \quad (1)$$

where $\varepsilon_{i\mathbf{k}} = s_i (\mathbf{k}^2/2m_i - \varepsilon_{F_i})$ is the parabolic dispersion of the i -th band with Fermi-energy ε_{F_i} and electron mass m_i . $s_i = \pm$ determines electron/hole-like character of the respective band. The intraband order parameter is self-consistently determined by the BCS equation $\Delta_i = \sum_{j\mathbf{k}} U_{ij} \langle c_{j-\mathbf{k}\downarrow} c_{j\mathbf{k}\uparrow} \rangle$. Interband pairing in BCS superconductors is considered weak (discussion, reference) and has been neglected in our model.

Order parameters of different bands are mixed by off-diagonal terms of the coupling matrix U_{ij} . In the present work, we parametrize gap-mixing by a parameter v and define

$$U_{ij} = \begin{pmatrix} U_{11} & vU_{11} \\ vU_{11} & U_{22} \end{pmatrix}$$

in the case of a two-band superconductor. For given Δ_i and v we can thus find U_{11} and U_{22} such that the gap equation is satisfied.

To model an experimental probe with a laser pulse, we introduce a time dependent gauge vector potential $\mathbf{A}(t) = \mathbf{e}A(t)$ by means of minimal coupling,

$$\mathcal{H}_1 = - \sum_{i\mathbf{k}\mathbf{k}'\sigma} \mathbf{J}_{i\mathbf{k}\mathbf{k}'} \cdot \mathbf{A} c_{i\mathbf{k}\sigma}^\dagger c_{i\mathbf{k}'\sigma} + \sum_{i\mathbf{k}\sigma} \frac{s_i e^2}{2m_i} \mathbf{A}^2 c_{i\mathbf{k}\sigma}^\dagger c_{i\mathbf{k}\sigma}.$$

$J_{i\mathbf{k}\mathbf{k}'} = \langle i\mathbf{k} | \frac{e\mathbf{P}_i}{m_i} | i\mathbf{k}' \rangle$ are intraband transition matrix elements of the current operator. (Discussion why we neglect interband transitions). The two terms in \mathcal{H}_1 corresponds to the paramagnetic and diamagnetic coupling to the laser field, respectively. The full Hamiltonian is given by $\mathcal{H} = \mathcal{H}_0 + \mathcal{H}_1$.

B. Impurity scattering

In a clean system momentum conservation yields $\mathbf{J}_{i\mathbf{k}\mathbf{k}'} \sim \delta_{\mathbf{k}\mathbf{k}'}$, or $\mathbf{J}_{i\mathbf{k}\mathbf{k}'} \sim \delta_{\mathbf{k}, \mathbf{k}' \pm \mathbf{q}}$ if a photon wavevector \mathbf{q} is considered. In disordered systems translational invariance is broken, so that transitions between states of different momentum are allowed. Here, we adopt the approach of Murotani and Shimano [1] and model the effects of impurities by means of the Mattis-Bardeen (MB) substitution [2]. It relies on approximating the transition matrix elements $J_{i\mathbf{k}\mathbf{k}'}$ as a Lorentzian in momentum

transfer space, explicitly written as

$$\langle |\mathbf{e} \cdot \mathbf{J}_{i\mathbf{k}\mathbf{k}'}|^2 \rangle_{\text{Av}} = \int \frac{d\Omega_{\mathbf{k}}}{4\pi} \frac{d\Omega'_{\mathbf{k}}}{4\pi} |\mathbf{e} \cdot \mathbf{J}_{i\mathbf{k}\mathbf{k}'}|^2 \quad (2)$$

$$\approx \frac{(ev_{F_i})^2}{3\pi N_i(0)} \frac{\gamma_i}{(\varepsilon_{i|\mathbf{k}|} - \varepsilon_{i|\mathbf{k}'|})^2 + \gamma_i^2}, \quad (3)$$

with Fermi velocity v_{F_i} density of states of the Fermi level $N_i(0)$ and impurity scattering rate γ_i . Note that we are considering an effectively one-dimensional quantity where all angular degrees of freedom have been averaged out. Physically, this means that impurity scattering occurs with equal probability between all states within a shell around the Fermi sphere. A derivation of this matrix element following [Murotani] is reviewed in Appendix A.

An optical transition can be resonantly driven only if (1) an energy matching condition and (2) a momentum matching condition is satisfied. Assuming a transition energy of Δ , condition (1) can be satisfied by tuning the optical pulse frequency to $\omega = \Delta$. Let us for simplicity consider a one-dimensional system. If Δ is sufficiently small, the parabolic dispersion can be linearized at the Fermi level, $\varepsilon_k = v_F k$. Then, a momentum of Δ/v_F is necessary to satisfy condition (2). In a clean system it then follows that photoexcitation within a single band is not possible if bandfolding effects are also neglected. In a weakly disordered system, momentum is no longer a good quantum number. Here, momentum broadening δk can be viewed as providing the necessary momentum and the transition becomes resonant for $v_F \delta k = \Delta$. For strong disorder the concept of momentum is lost and any two states can be connected by satisfying condition (1) only.

In the MB approximation, \mathbf{k} is still treated as an exact quantum number of the unperturbed system but presence of impurities broadens momentum conservation of the transition matrix element $\mathbf{J}_{i\mathbf{k}\mathbf{k}'}$ into a Lorentzian momentum transfer distribution of width γ_i centered at zero momentum transfer. It is straightforward to check that for an excitation of energy Δ the matrix element gives the largest contribution for an impurity scattering rate of $\gamma_i = \Delta$.

One may picture the Higgs excitation as a two-photon excitation process, where the first photon populates a virtual intermediate state at energy Δ above the groundstate and the second photon contributes the remaining Δ to establish resonance with the Higgs mode at 2Δ . Based on these arguments, we can expect the largest enhancement of the Higgs resonance at $\gamma_i = \Delta$.

[Discussion of relevant scales $\Delta, \gamma, \omega_D, \varepsilon_F$. Specifically, what happens when $\gamma > \omega_D$?]

C. Equations of motion

We solve for the time dynamics of above Hamiltonian using a density matrix approach. To this end, we define the density matrix $\rho = |\psi_0\rangle\langle\psi_0|$, or, in the basis of single-

particle/hole excitations, $\mathcal{B} = \{c_{i\mathbf{k}\uparrow}|0\rangle, c_{i-\mathbf{k}\downarrow}|0\rangle\}$

$$\rho = \begin{pmatrix} \rho_{i\mathbf{k}\mathbf{k}'}^{11} & \rho_{i\mathbf{k}\mathbf{k}'}^{12} \\ \rho_{i\mathbf{k}\mathbf{k}'}^{21} & \rho_{i\mathbf{k}\mathbf{k}'}^{22} \end{pmatrix} = \begin{pmatrix} \langle c_{i\mathbf{k}\uparrow}^\dagger c_{i\mathbf{k}'\uparrow} \rangle & \langle c_{i\mathbf{k}\uparrow}^\dagger c_{i-\mathbf{k}'\downarrow}^\dagger \rangle \\ \langle c_{i-\mathbf{k}\downarrow} c_{i\mathbf{k}'\uparrow} \rangle & \langle c_{i-\mathbf{k}\downarrow} c_{i-\mathbf{k}'\downarrow}^\dagger \rangle \end{pmatrix}$$

The time dependence of ρ is given by the Heisenberg equation of motion,

$$i\partial_t \rho = [\rho, H]$$

where H is the operator \mathcal{H} in the basis \mathcal{B} .

We are interested in computing the dynamics of the current $\mathbf{j} = -\langle \frac{\delta \mathcal{H}}{\delta \mathbf{A}} \rangle = \mathbf{j}_P + \mathbf{j}_D$, consisting of a paramagnetic and diamagnetic contribution,

$$\begin{aligned} \mathbf{j}_P &= \sum_{i\mathbf{k}\mathbf{k}'} \mathbf{J}_{i\mathbf{k}\mathbf{k}'} (\rho_{i\mathbf{k}\mathbf{k}'}^{11} - \rho_{i\mathbf{k}\mathbf{k}'}^{22} + 1) \\ \mathbf{j}_D &= - \sum_{i\mathbf{k}\sigma} \frac{s_i e^2}{2m_i} \mathbf{A} (\rho_{i\mathbf{k}\mathbf{k}'}^{11} - \rho_{i\mathbf{k}\mathbf{k}'}^{22} + 1) \end{aligned}$$

and we compute the dynamics of the superconducting order parameter

$$\Delta_i = \sum_{j\mathbf{k}} U_{ij} \rho_{j\mathbf{k}\mathbf{k}}^{21}.$$

To apply the MB substitution we further expand above equation of motions in orders of $A(t)$. To account for effects of a THG response, we consider terms up to third order. As detailed in Appendix B, the current only has odd order components $\mathbf{j} = \mathbf{j}|_0 + \mathbf{j}|_3 + \dots$ and the gap only contains even contributions of A , $\Delta = \Delta|_0 + \Delta|_2 + \dots$.

Finally, we exploit the rotational invariance of our model and perform the integral over angular degrees of freedom explicitly. Thus, by replacing all momentum summations by an integral $\sum_{\mathbf{k}} \rightarrow N_i(0) \int d\varepsilon_{i\mathbf{k}} \int \frac{d\Omega_{\mathbf{k}}}{4\pi}$, we effectively reduce the model to a one-dimensional system. Note that rotational invariance of our continuum model neglects polarization dependence of observable quantities.

We are left to compute the equations of motion of the angle-averaged quantities

$$\begin{aligned} R_{\varepsilon_{|\mathbf{k}|}}^{1/3,n} &= \int \frac{d\Omega_{\mathbf{k}}}{4\pi} \int \frac{d\Omega_{\mathbf{k}'}}{4\pi} \mathbf{J}_{i\mathbf{k}\mathbf{k}'} \rho_{i\mathbf{k}\mathbf{k}'}^{nn} |_{1/3} \\ r_{\varepsilon_{|\mathbf{k}|}}^{nm} &= \int \frac{d\Omega_{\mathbf{k}}}{4\pi} \rho_{i\mathbf{k}\mathbf{k}'}^{nm} |_2. \end{aligned}$$

We solve them numerically using a [Runge-Kutta] solver on a discretized energy grid $\varepsilon_{|\mathbf{k}_i|}$ of up to 10^3 points in the interval $[-\omega_D, \omega_D]$ (why do we use ω_D ??). A detailed derivation and an explicit presentation of the full equations of motion is given in Appendix B.

III. SINGLE-BAND SUPERCONDUCTIVITY

Motivated by the experiment of Matsunaga et al. [] we choose parameters $\Delta_{\text{eq}} = 1.3 \text{ meV}$, $\varepsilon_F = 1 \text{ eV}$, $m = 0.78m_e$, $s = 1$ that reflect measurements and ab-initio

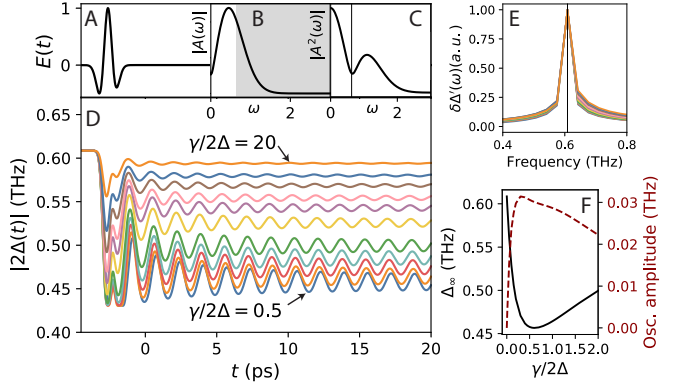


Figure 1. (a) Pulse field $E(t)$ realizing a quench. (b) Spectral composition $|A(\omega)|$. The gray shaded area illustrates the quasi-particle continuum. (c) Spectral compositon $A^2(\omega)$ of the second order component $A^2(t)$ responsible for excitation of collective modes. The peak around zero frequency corresponds to a DFG process while the peak at finite 1.2 THz is a SFC process. (d) Evolution of the magnitude of the order parameter $|2\Delta(t)|$ for impurity strength varying from $\gamma/2\Delta = 0.5$ to 20 and Fourier spectrum of the gap oscillations (d). (e) Relaxation value Δ_∞ and amplitude of oscillation show a very similar dependence as a function of disorder strength which has maximum effect at around $\gamma \approx \Delta$.

calculations on NbN [DFT-reference]. The Debye energy for NbN is order order of $\omega_D = 50 \text{ meV}$, but for better numerical resolvability we choose $\omega_D = 20 \text{ meV}$.

We choose the electromagnetic pulse form $A(t) = A_0 \exp(-(t-t')^2/2\tau^2) \cos \Omega t$ and choose coefficients to match the reported data of [Matsunaga]. The resulting electrical field waveform is shown in Fig. 1(a).

A characteristic property of a pump pulse is its pulse length τ compared to the natural timescale of the superconductor, $1/\Delta$. For $\tau \ll \hbar/\Delta$ the superconductor is *quenched*, while it is *adiabatically driven* in the opposite limit of $\tau \gg 1/\Delta$. The different behavior in the two limits can be intuitively understood from the simple relation

$$\delta\Delta(\omega) \sim K(\omega) A^2(\omega)$$

where $K(\omega)$ is the optical nonlinear kernel []. Presence of a collective mode translates into a peak of the optical Kernel at the characteristic mode energy $\omega = 2\Delta$, illustrated in Fig. 1(c) by a vertical line. $A^2(\omega)$ is the Fourier transform of the squared vector potential $A(t)^2$ and hence given by a self-convolution of $A(\omega)$. $A^2(\omega)$, shown in Fig. 1(c), has a double-peaked structure. The first peak, centered at $\omega = 0$, corresponds to a difference frequency process (DFG), while the second peak at $\omega = 2\Omega$ corresponds to a sum frequency process (SFG). For $\Delta\tau \ll 1$, the frequency structure of $A^2(\omega)$ is very broad. The response of $\delta\Delta(\omega)$ is then dominated by the sharp resonance peak of $K(\omega)$ giving rise to pronounced 2Δ -oscillations of the superconducting gap in the time domain. Since the DFG peak is guaranteed to overlap with the Higgs resonance, these oscillations will always be present, independent of the frequency of the optical pulse. The SFG process only

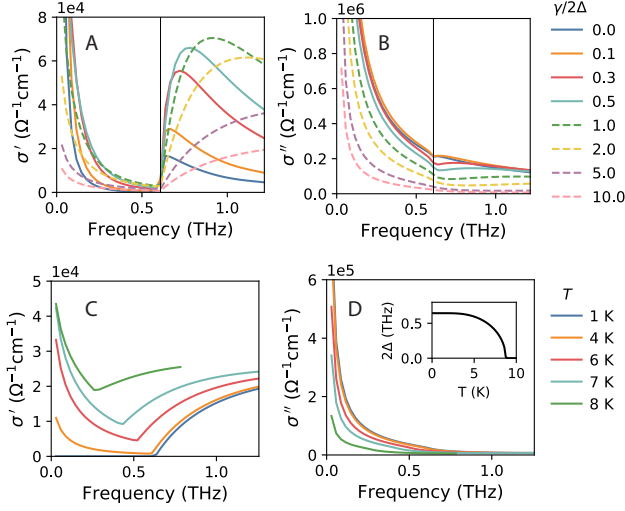


Figure 2. Real part σ' (A,C) and imaginary part σ'' (B,D) of optical conductivities to first order in A for various impurity scattering rates at $T = 4\text{ K}$ (A,B) and various temperatures at $\gamma/2\Delta = 10$. σ' show a characteristic conductivity gap below T_C and both σ', σ'' diverge in the static limit.

contributes if the pulse frequency lies in the vicinity of $\Omega \approx \Delta$.

In the transient limit, $\Delta\tau \gg 1$, the frequency structure of $\delta\Delta(\omega)$ is dominated by the sharp SFG peak of the pulse. The gap will show a forced oscillation with frequency 2Ω which, however, is resonantly enhanced when $2\Omega \approx 2\Delta$.

Following Matsunaga, we choose a pulse with $\Delta\tau = 0.x$, closest to the quench scenario. The superconducting order parameter indeed shows characteristic oscillations with frequency $2\Delta = \Delta_{\text{eq}}$ as shown in Figs. 1(d-e). The gap can be seen to respond to the THz pulse by a marked drop followed by damped oscillations around a new value Δ_∞ . $|\Delta^{eq} - \Delta_\infty| \propto \int d\omega \sigma'(\omega) A(\omega)$. Discussion why it does not oscillate with Δ_∞

Both the oscillation amplitude and Δ_∞ show a strong dependence on the impurity scattering rate peaked at $\gamma \approx \Delta^{eq}$, see Fig. 1(f). For $\gamma \rightarrow 0$ the Higgs resonance vanishes. [Discussion photon \mathbf{q} and A^2 term] These results underline the importance of impurity scattering for the excitation efficiency of collective Higgs modes uncovered recently [6]. We can understand this result by examining the matrix elements of the current operator, Eq. (3), following the discussion of Sec. II B. Indeed, the γ -dependence closely follows the functional form $\gamma/(\Delta_{eq}^2 + \gamma^2)$.

Next we compute the optical conductivity in linear response

$$\sigma_0(\omega) = \frac{j(\omega)|_1}{i\omega A(\omega)}.$$

Real and imaginary parts $\sigma'(\omega), \sigma''(\omega)$ are plotted in Fig. 2(a-b) for various impurity concentrations and in Fig. 2 for various temperatures. At low temperatures σ' shows a clear conductivity gap below $2\Delta^{eq}$. In the clean

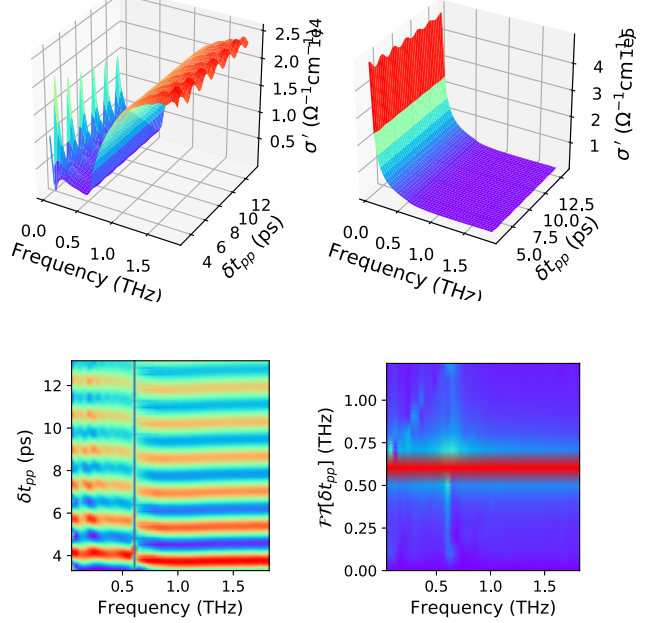


Figure 3. (A,B) Conductivity spectra for swept pump-probe delay δt_{p-p} to third order in A . (C) False-color plot of σ' which was average-subtracted and normalized to show the oscillations. A phase shift occurs across the resonance at $2\Delta_{\text{eq}}$ of the quench pulse frequency. (D) Fourier spectrum of panel (C) showing that frequency of conductivity oscillation is peaked at $2\Delta_{\text{eq}}$.

limit, a pronounced coherence peak is observed around 2Δ , reflecting the additional density of states amassed above the quasiparticle gap. The above-gap absorption reaches a maximum at $\gamma \sim 2\Delta$ and broadens into the characteristic dome shape for which the original analytical MB expression has been derived [6]. In the $T \rightarrow 0$ limit, the conductivity shows a condensate peak $\sigma'(\omega) = \delta(\omega)$ below the gap which is broadened at finite temperatures.

Higher orders of the optical conductivity include contributions of collective modes that smooth out the absorption edge and add spectral weight inside the conductivity gap. Here, we calculate the non-linear contribution,

$$\sigma(\omega, \delta t_{pp}) = \frac{j(\omega)|_1 + j(\omega)|_3}{i\omega A(\omega)},$$

in a pump-probe setting. To this end, we pump the system with an intense pulse of fluence $A = X$ and after a delay of δt_{pp} , apply a probe pulse. Following experimental schemes [6], we perform two simulations modelling both pump and probe, j_{p-p} , and a pump only j_p . We then compute the optical conductivity from the difference in currents $j = j_{p-p} - j_p$. This ensures that resilient components of the pump do not contribute to the optical conductivity.

Figures 3(a-b) show the real and imaginary part of the optical conductivity $\sigma(\omega, \delta t_{pp})$ as a function of frequency and pump-probe delay. It can be seen that the additive

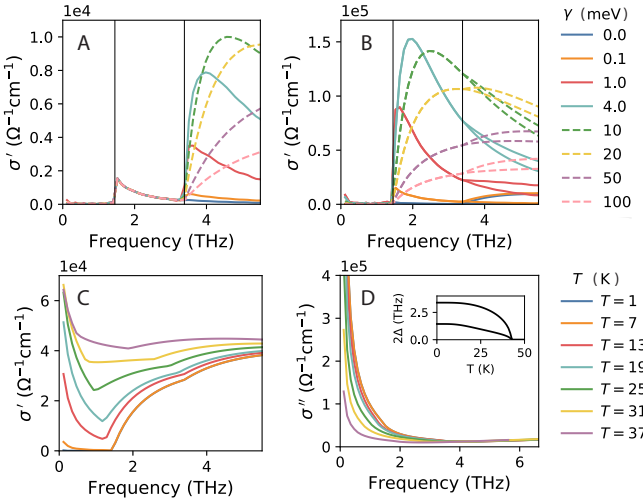


Figure 4. Real part σ' (a,c) and imaginary part σ'' (b,d) of optical conductivities to first order in A for various impurity scattering rates at $T = 4\text{ K}$ (A,B) and various temperatures at $\gamma/2\Delta = 10$. σ' show a characteristic conductivity gap below T_C and both σ', σ'' diverges as $1/\omega$ in the static limit.

third-order contribution $j|_3$ add spectral weight to the conductivity that slightly fills the absorption gap. These contributions show clear oscillations for all frequencies ω , as can be seen from Fig. 3(c) where the dome-shaped envelope has been subtracted. A Fourier transform of these oscillations is shown in Fig. 3(e) indicating that the oscillation frequency matches $2\Delta^{eq}$, the resonance frequency of the Higgs mode. Our results show that signatures of the Higgs mode are measurable in the pump-probe response of the optical conductivity. All features are resolvable by present-day experimental techniques. [Discuss agreement with experiment]

IV. MULTI-BAND SUPERCONDUCTIVITY

Motivation by the good agreement of the theory with experimental data, we now discuss the case of a two-band superconductor. Here, the superconducting state of MgB₂ is likely the most widely studied example and we adopt it as a reference material. We loosely model the π - and σ -bands believed to be responsible for superconductivity by choosing material parameters $\Delta_\pi = 3\text{ meV}$, $\Delta_\sigma = 7\text{ meV}$, $\varepsilon_{F,\pi} = 2.9\text{ eV}$, $\varepsilon_{F,\sigma} = 0.7\text{ eV}$, $m_\pi = 0.85m_e$, $m_\sigma = 1.38m_e$, $\omega_D = 50\text{ meV}$, $s_\pi = 1$, $s_\sigma = -1$.

A. Optical conductivity

B. Leggett mode and THG

- Definition, equation of Leggett mode

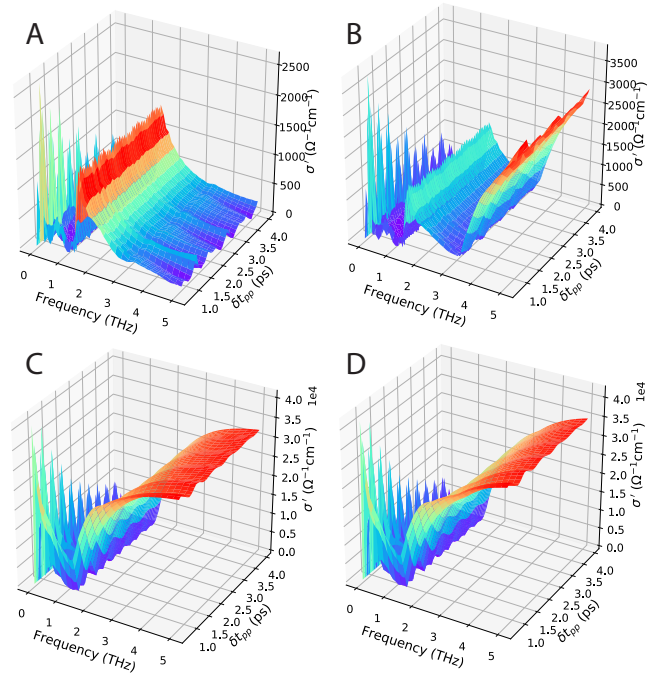


Figure 5. Time-resolved optical conductivity for the case were bands are in the limit (a) clean-clean, (b) clean-dirty, (c) dirty-clean, (d) dirty-dirty.

- Leggett equation of motion (equation for imaginary part of gap) completely decouples from the remaining system of equations!
- In light of this - does Leggett mode really couple with Higgs mode? Here the issue of the Fourier-transform comes up again. Is it possible that the Fourier-transform of the whole time-range is the correct approach. A point is that Leggett mode is peaked in between the two gaps, but all oscillation contributions above $2\Delta_1$ are damped very fast (exponential) so that at later times it looks like the energy of the mode is $2\Delta_1$.
- TGH experiment. Here, let's decompose the THG signal in quasiparticle, Higgs, Leggett contributions and show the THG in two ways. First, a plot as a function of frequency for the four impurity cases. Second, a plot as a function of temperature for the four cases. The two plots should agree qualitatively, since changing the temperature changes the gap (this is what experimentalists do). Additionally, however, thermal effects contribute which might make things a bit harder to see.
- Discuss Fig. 5 for varying coupling strength and compare with clean limit result

Leggett mode has been potentially measured in between the two gaps. Discuss this and also refer to Schnyder Nature Comm.

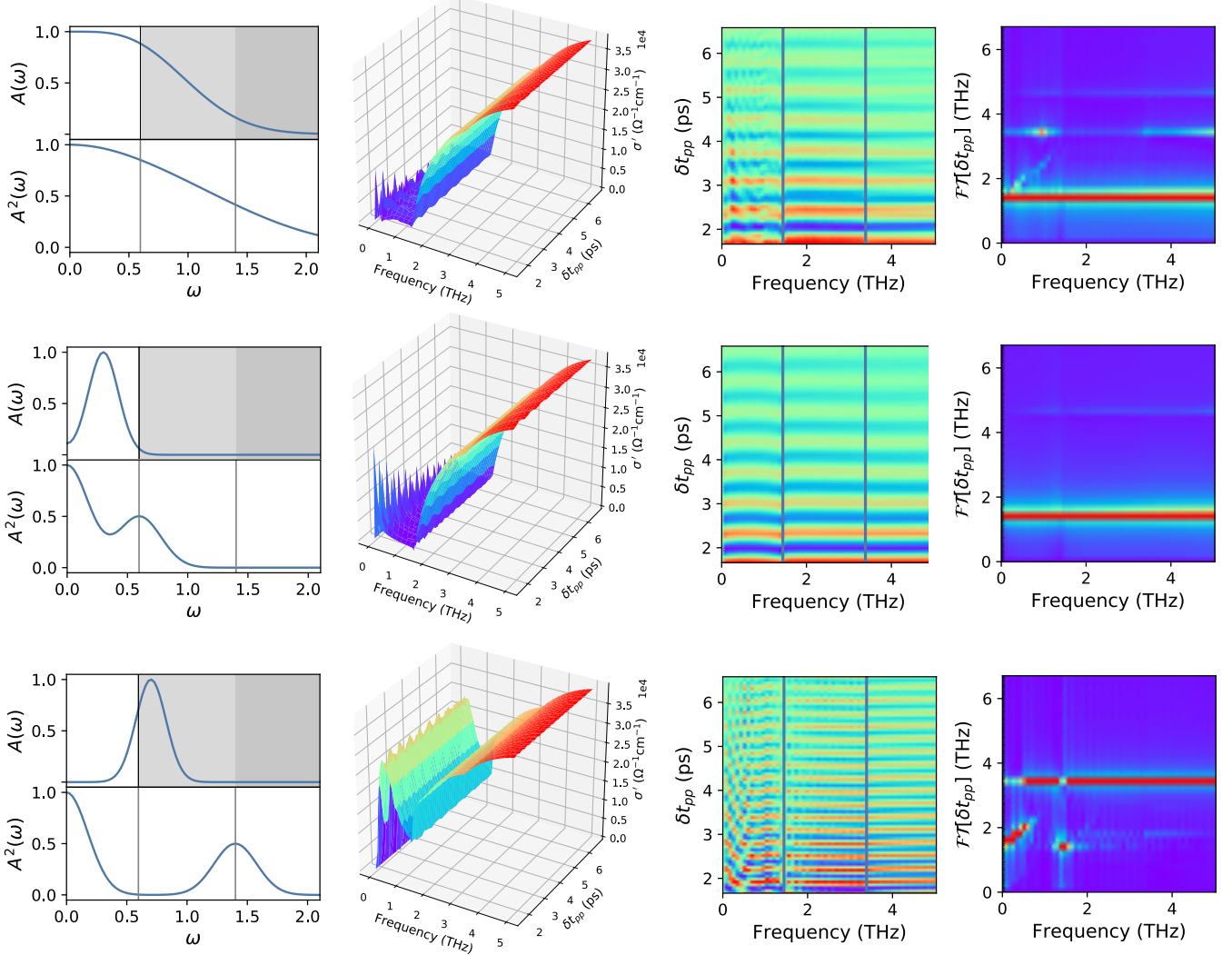


Figure 6. Time-resolved optical conductivity for three different pulses.

V. CONCLUSION

...

ACKNOWLEDGMENTS

...

Appendix A: Mattis-Bardeen substitution

One starts with the following assumption:

$$\rho_k(R) = \langle \phi_{\mathbf{k}}^*(\mathbf{r}) \phi_{\mathbf{k}}(\mathbf{r}') \rangle_{Av} = \frac{\sin kR}{kR} e^{-R/2l}$$

where $R = |\mathbf{r} - \mathbf{r}'|$ and $\langle \cdot \rangle_{Av} = \int \frac{d\Omega_{\mathbf{k}}}{4\pi} (\cdot)$ denotes averaging over the angle of \mathbf{k} . l is the mean-free path.

$$\begin{aligned}
 & \langle |J_{\mathbf{k}\mathbf{k}'}^i|^2 \rangle_{Av} \\
 &= \frac{e^2}{m^2} \left| \int d^3\mathbf{r} \phi_{\mathbf{k}}^*(\mathbf{r}) \frac{\partial_i}{i} \phi_{\mathbf{k}'}(\mathbf{r}) \right|^2 \\
 &= \frac{e^2}{m^2} \int \int \frac{d\Omega_{\mathbf{k}}}{4\pi} \frac{d\Omega_{\mathbf{k}'}}{4\pi} \int d^3\mathbf{r} \phi_{\mathbf{k}}^*(\mathbf{r}) \frac{\partial_i}{i} \phi_{\mathbf{k}'}(\mathbf{r}) \int d^3\mathbf{r}' \phi_{\mathbf{k}}(\mathbf{r}') \frac{\partial'_i}{i} \phi_{\mathbf{k}'}^*(\mathbf{r}') \\
 &= \frac{e^2}{m^2} \int \int \frac{d\Omega_{\mathbf{k}}}{4\pi} \frac{d\Omega_{\mathbf{k}'}}{4\pi} \int d^3\mathbf{r} \phi_{\mathbf{k}}^*(\mathbf{r}) \frac{\partial_i}{i} \phi_{\mathbf{k}'}(\mathbf{r}) \int d^3\mathbf{r}' \left(-\frac{\partial'_i}{i} \phi_{\mathbf{k}}(\mathbf{r}') \right) \phi_{\mathbf{k}'}^*(\mathbf{r}') \\
 &= \frac{e^2}{m^2} \int d^3\mathbf{r} d^3\mathbf{r}' \int \frac{d\Omega_{\mathbf{k}}}{4\pi} \phi_{\mathbf{k}}^*(\mathbf{r}) \partial'_i \phi_{\mathbf{k}}(\mathbf{r}') \int \frac{d\Omega_{\mathbf{k}'}}{4\pi} \phi_{\mathbf{k}'}^*(\mathbf{r}') \partial_i \phi_{\mathbf{k}'}(\mathbf{r}) \\
 &= \frac{e^2}{m^2} \int d^3\mathbf{r} d^3\mathbf{r}' \partial'_i \langle \phi_{\mathbf{k}}^*(\mathbf{r}) \phi_{\mathbf{k}}(\mathbf{r}') \rangle_{Av} \partial_i \langle \phi_{\mathbf{k}'}^*(\mathbf{r}') \phi_{\mathbf{k}'}(\mathbf{r}) \rangle_{Av} \\
 &= \frac{e^2}{m^2} V \int d^3\mathbf{R} \frac{\partial \rho_k(R)}{\partial R} \frac{\partial \rho_{k'}(R)}{\partial R}
 \end{aligned}$$

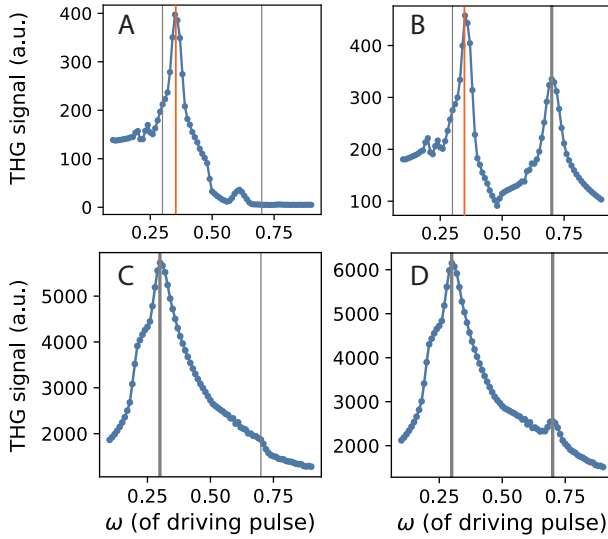


Figure 7. Caption

Now we make use of the fact that

$$\int_0^{2\pi} d\varphi \int_0^\pi d\theta \sin \theta \frac{R_i^2}{R^2} = \frac{4\pi}{3}$$

We see that the expression is now independent of the component index i of the real-space vector $\mathbf{J}_{kk'}$. This means that averaging over angles in momentum space results in loss of polarization dependence in real-space.

Performing the remaining integral gives

$$\begin{aligned} \langle |J_{kk'}^i|^2 \rangle_{Av} &= \frac{2\pi}{3} \frac{e^2}{m^2} V \int_0^\infty dR e^{-R/l} \cos(k - k') R \\ &= \frac{2\pi}{3} \frac{e^2}{m^2} V \frac{1/l}{(1/l)^2 + (k - k')^2} \end{aligned}$$

Close to the Fermi surface we have $\varepsilon_{\mathbf{k}} = v_F(k - k_F)$ which yields

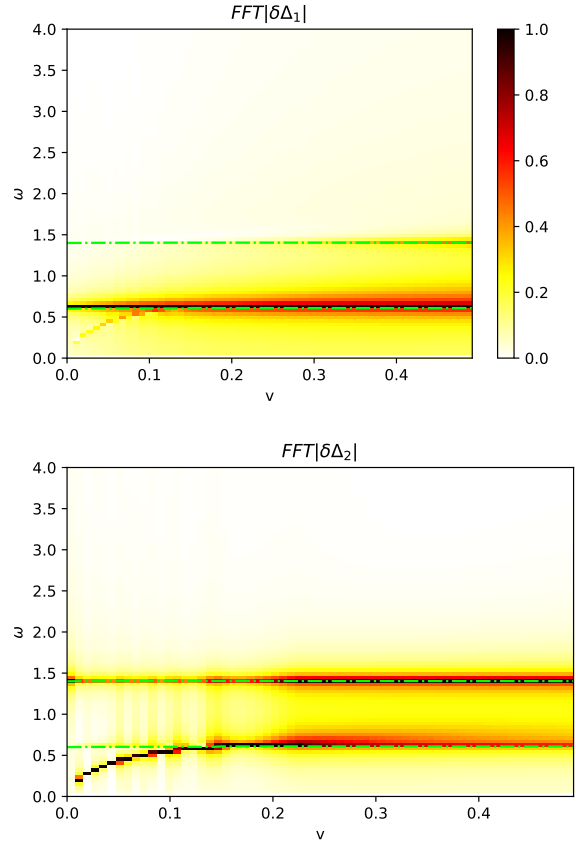
$$\langle |J_{kk'}^i|^2 \rangle_{Av} = \frac{2\pi}{3} \frac{e^2}{m^2} V \frac{1/l}{(1/l)^2 + (\varepsilon_k - \varepsilon_{k'})^2/v_F^2}$$

Appendix B: Model

$$\mathcal{H}_0 = \sum_{i\mathbf{k}\sigma} \varepsilon_{i\mathbf{k}} c_{i\mathbf{k}\sigma}^\dagger c_{i\mathbf{k}\sigma} + \sum_{i\mathbf{k}} \left(\Delta_i c_{i-\mathbf{k}\uparrow}^\dagger c_{i\mathbf{k}\downarrow}^\dagger \right), \quad (B1)$$

where $\varepsilon_{i\mathbf{k}} = s_i (\mathbf{k}^2/2m_i - \varepsilon_{F_i})$ and the superconducting order parameter is self-consistently determined by $\Delta_i = \sum_{j\mathbf{k}} U_{ij} \langle c_{j-\mathbf{k}\downarrow} c_{j\mathbf{k}\uparrow} \rangle$.

$$\mathcal{H}_1 = - \sum_{i\mathbf{k}\mathbf{k}'\sigma} \mathbf{J}_{i\mathbf{k}\mathbf{k}'} \cdot \mathbf{A} c_{i\mathbf{k}\sigma}^\dagger c_{i\mathbf{k}'\sigma} + \sum_{i\mathbf{k}\sigma} \frac{s_i e^2}{2m_i} \mathbf{A}^2 c_{i\mathbf{k}\sigma}^\dagger c_{i\mathbf{k}\sigma}$$



$$\begin{aligned} \langle |\mathbf{e} \cdot \mathbf{J}_{i\mathbf{k}\mathbf{k}'}|^2 \rangle_{Av} &= \int \frac{d\Omega_{\mathbf{k}}}{4\pi} \frac{d\Omega'_{\mathbf{k}}}{4\pi} |\mathbf{e} \cdot \mathbf{J}_{i\mathbf{k}\mathbf{k}'}|^2 \\ &\approx \frac{(ev_{F_i})^2}{3\pi N_i(0)} \frac{\gamma_i}{(\varepsilon - \varepsilon')^2 + \gamma_i^2} \end{aligned}$$

Discussion of A, A^2 .

The full Hamiltonian is given by $\mathcal{H} = \mathcal{H}_0 + \mathcal{H}_1$.

$$\mathbf{j} = - \left\langle \frac{\delta \mathcal{H}}{\delta \mathbf{A}} \right\rangle = \mathbf{j}_P + \mathbf{j}_D$$

$$\mathbf{j}_P = \sum_{i\mathbf{k}\mathbf{k}'\sigma} \mathbf{J}_{i\mathbf{k}\mathbf{k}'} \cdot \mathbf{A} \langle c_{i\mathbf{k}\sigma}^\dagger c_{i\mathbf{k}'\sigma} \rangle$$

$$\mathbf{j}_D = - \sum_{i\mathbf{k}\sigma} \frac{s_i e^2}{2m_i} \mathbf{A} \langle c_{i\mathbf{k}\sigma}^\dagger c_{i\mathbf{k}\sigma} \rangle$$

Next we construct the density matrix

$$\rho = |\psi_0\rangle \langle \psi_0| = \begin{pmatrix} \rho_{11}^{11} & \rho_{12}^{12} \\ \rho_{21}^{21} & \rho_{22}^{22} \end{pmatrix} = \begin{pmatrix} \langle c_{i\mathbf{k}\uparrow}^\dagger c_{i\mathbf{k}'\uparrow} \rangle & \langle c_{i\mathbf{k}\uparrow}^\dagger c_{i-\mathbf{k}'\downarrow}^\dagger \rangle \\ \langle c_{i-\mathbf{k}\downarrow} c_{i\mathbf{k}'\uparrow} \rangle & \langle c_{i-\mathbf{k}\downarrow} c_{i-\mathbf{k}'\downarrow} \rangle \end{pmatrix}$$

